

Origin of giant valley splitting in silicon quantum wells induced by superlattice barriers

Gang Wang^{1,2}, Zhi-Gang Song^{1,*}, Jun-Wei Luo,^{1,2,3,†} and Shu-Shen Li^{1,2}

¹State Key Laboratory of Superlattices and Microstructures, Institute of Semiconductors, Chinese Academy of Sciences, Beijing 100083, China

²Center of Materials Science and Optoelectronics Engineering, University of Chinese Academy of Sciences, Beijing 100049, China

³Beijing Academy of Quantum Information Sciences, Beijing 100193, China

 (Received 21 October 2021; revised 13 February 2022; accepted 31 March 2022; published 21 April 2022)

Enhancing valley splitting in SiGe heterostructures is crucial for developing silicon spin qubits. Complex SiGe heterostructures, sharing a common feature of four-monolayer (4 ML) Ge layer next immediately to the silicon quantum well (QW), have been computationally designed in 2013 to have giant valley splitting approaching 9 meV and hence could be used to overcome the challenge of valley splitting towards the experimental realization of Si quantum computing. However, none of them has been successfully fabricated, perhaps due to their complexity. Here, we remarkably simplify the originally designed complex SiGe heterostructures by laying out the Si QW directly on the SiGe substrate followed by capping a $(\text{Ge}_4\text{Si}_4)_n$ superlattice (SL) barrier with a sacrifice in valley splitting (VS), which is reduced from a maximum value of 8.7 to 5.2 meV. Even the smallest number of SL periods ($n = 1$) will also give a sizable VS of 1.6 meV, which is large enough for developing stable spin qubits. We further develop an effective Hamiltonian model to reveal the physical mechanism underlying the enhanced valley splitting by the $(\text{Ge}_4\text{Si}_4)_n$ SL barriers. We surprisingly find that the presence of the SL barrier will reduce rather than enhance the VS in most cases. The only exception is the $(\text{Ge}_4\text{Si}_4)_n$ SL barriers, where their miniband states have such a strong coupling with Si QW valley states that they provide an even larger VS. These findings lay a solid theoretical foundation for overcoming the valley splitting issue of SiGe heterostructures in the experiment that is heading toward Si quantum computing.

DOI: [10.1103/PhysRevB.105.165308](https://doi.org/10.1103/PhysRevB.105.165308)

I. INTRODUCTION

Silicon spin qubits have several advantages over other competing qubit schemes [1,2] including extremely long spin relaxation time [3] and dephasing time [1], the scalability, and the mature microelectronic technologies [2]. Particularly, the last one is the key advantage for its capability to integrate both the qubits and electronics on a single chip to take advantage of both spin and charge degrees of freedom of electrons and fabricate millions of qubits in a silicon quantum chip needed to implement universal quantum computing. However, the electronic energy level is twofold degenerate in Si quantum dots due to the sixfold degenerate bulk Si conduction band X-valleys, which becomes a primary factor hindering us from achieving the well-defined and effectively controlled silicon spin qubits [1,2,4]. In bulk Si, the conduction band minimum is located at Δ point, $0.85 \times (2\pi/a_0)$ from the Γ point toward the X point of the Brillouin zone ($a_0 = 5.43 \text{ \AA}$ is the Si lattice constant), and thus has a sixfold valley degeneracy. In Si quantum wells (QWs), the space confinement along the growth direction splits the sixfold degenerate Δ_6 valleys into a low-lying two-fold degenerate Δ_2 valley and a high-lying fourfold degenerate Δ_4 valley. The twofold degeneracy of the low-lying Δ_2 valley is difficult to be further lifted. For a system with its ground-state manifold is composed of more

than one orbital level, it is difficult to precisely manipulate the spin qubit and realize well-characterized qubits, which is one of the crucial criteria for the implementation of quantum computation [5]. In Si QWs, it was believed [6–11] that the sharp interfacial potential causes coupling between two low-lying Δ_2 valleys and thus lifts the twofold degeneracy with an energy separation referring to valley splitting (VS). The VS has to be much larger than the magnetic field-induced spin splitting (Zeeman splitting) to realize stable qubits. Numerous studies [12–15] have been carried out to evaluate the impacts of VS on the initialization and manipulation of Si spin qubits as well as to enhance the VS. For instance, it has been illustrated that for Si spin qubits, the VS magnitude determines the highest possible operation temperature, which is usually less than 30 mK [16–18] and was recently promoted to exceed 1 K [19,20]. Spin relaxation hotspots (peak in relaxation rate or rapid decline in the spin lifetime) occur when the VS equals the Zeeman splitting, indicating the VS must be large enough to exceed the Zeeman splitting to achieve a long spin lifetime [12,13]. Last but not least, sizable VS is also essential for the accomplishment of the two-electron qubits [21–23]. Unfortunately, in Si qubit devices the achievable VS is remarkably limited [12,24–31] to about $0.1 \sim 0.7$ meV in Metal-Oxide-Silicon (MOS) (Si/SiO₂) architecture [12,24] and to an even smaller range from 0.01 to 0.2 meV in Si/SiGe QW architecture [25–31].

Previous work [32], in the spirit of the inverse design [33,34] approach, has computationally designed Si QWs with substantially enhanced VS approaching 9 meV

*songzhigang@semi.ac.cn

†jwluo@semi.ac.cn

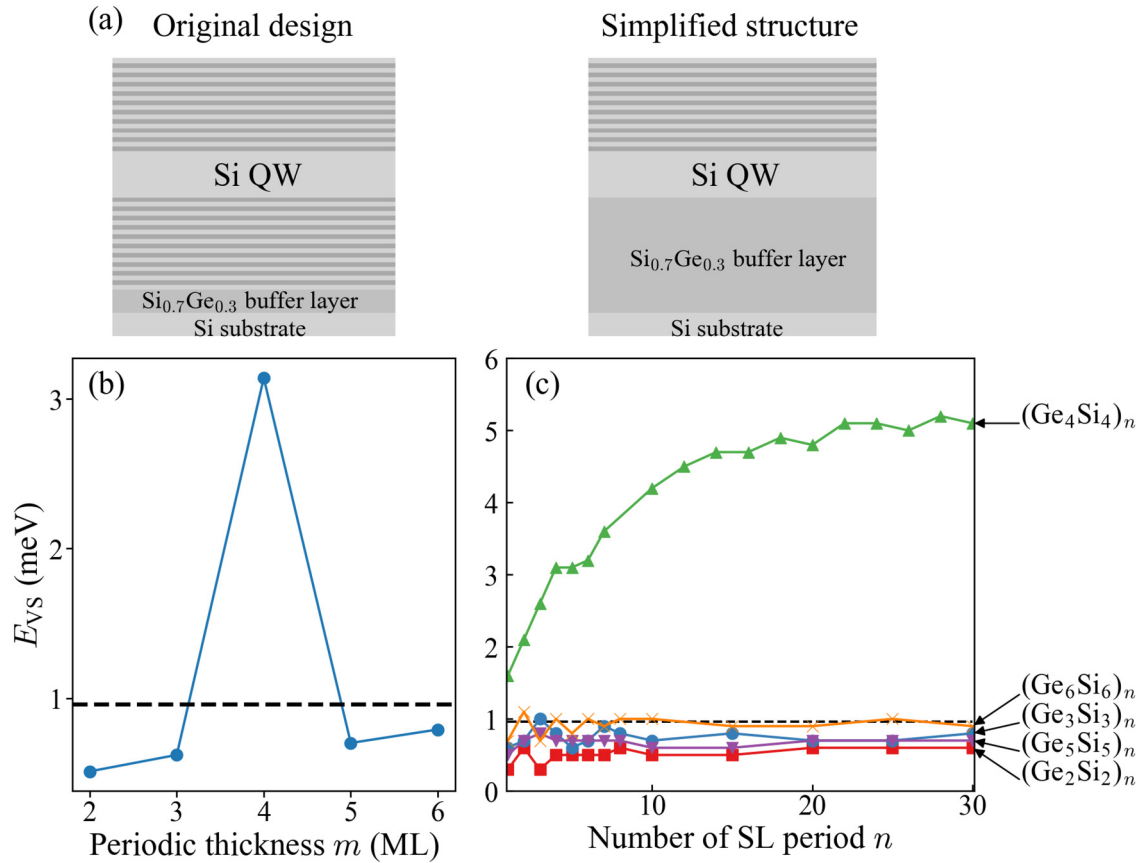


FIG. 1. (a) Schematic sketch of Si QW structure in the original design (left) and simplified Si QW structure in this work (right). (b) Computationally predicted VS of Si₄₀ QW/(Ge_{*m*}Si_{*m*})₄ SL barrier hybrid systems as varying period thickness m from 2 to 6 by performing atomistic SEMP calculations. The dashed horizon line marks the VS of the corresponding isolated 40-ML Si QW embedded in the pure Ge barrier. (c) Computationally predicted E_{VS} of Si₄₀ QW/(Ge_{*m*}Si_{*m*})_{*n*} SL barrier hybrid systems as a function of the number of SL periods n for period thickness $m = 2, 3, 4, 5, 6$.

relying on a combination of a genetic algorithm used to explore the Ge/Si superlattice (SL) barriers and atomistic semiempirical pseudopotential method (SEPM) for band structure calculations [35–37]. The searching configuration space comprises a thickness fixed Si QW (say 40 ML, 1 ML = $a_0/4$, a_0 is the lattice constant) sandwiched between two mirror-symmetric 80-ML thick Ge/Si SLs with varying the stacking sequence of Ge and/or Si monolayers. For a 40-ML thick Si QW, the optimized best SL barriers to have the largest VS are with stacking sequences of Ge₄Si₄Ge₂Si₆Ge₄Si₄Ge₄Si₂..., Ge₄Si₄Ge₄Si₂Ge₄Si₆Ge₄Si₂..., and Ge₄Si₆Ge₂Si₆Ge₄Si₄Ge₄Si₄... (subscript numbers denote the number of MLs and “...” represents the repetition of the preceding stacking) starting from the interface of 40-ML Si QW layer for substrates of pure Si and Si_{0.8}Ge_{0.2} and Si_{0.6}Ge_{0.4} alloys, respectively. The corresponding VS is 5.7, 7.4, and 8.7 meV, respectively. Interestingly, all designed SL barriers share the same feature as a 4-ML Ge sublayer immediately next to the 40-ML Si QW layer. Even a simple (Ge₄Si₄)₁₀ SL (10 periods with a repeating unit of 4-ML Ge/4-ML Si) barrier gives rise to a remarkably large VS of $E_{VS} = 7.2$ meV for 40-ML thick Si QW. By contrast, all explored SL barriers starting from a non-4-ML Ge sublayer afford a much smaller VS for Si QWs [32].

Although these computationally designed SL barriers offer one order of magnitude enhancement in VS for Si QWs, none of them has been fabricated to overcome the challenge of valley splitting towards Si quantum computing. Their complex stacking sequence or large SL periods might cause difficulties in fabrication. It is thus highly desired to simplify their structures to make them readily accessible to experimentalists utilizing currently reliable technology. Particularly, a thinner SL barrier will help improve gate voltage control since spin qubits in gate-defined Si quantum dots (QDs) are electrically insulated from top metal gates by a gate oxide insulating layer and the SiGe barrier layer. It is also interesting to unravel the physics underlying the interface engineering to achieve an order of magnitude enhancement in VS for Si QWs.

This work aims to simplify the structures to make them feasible for fabrication and reveal the physics governing the VS enhancement by the (Ge₄Si₄)_{*n*} SL barriers for Si QWs. Specifically, we consider putting the Si QW directly on the Si_{0.7}Ge_{0.3} substrate followed by a capping layer of a Ge/Si SL [schematically shown in Fig. 1(a)] instead of sandwiching the Si QW between two mirror-symmetric Ge/Si SLs [schematically shown in Fig. 1(a)] in the original design [32]. We name such simplified structures as Si₄₀ QW/(Ge_{*m*}Si_{*m*})_{*n*}; SL barrier hybrid systems hereafter. Note that to simplify the atomistic

calculations and analysis, we make an approximation for the substrate by replacing $\text{Si}_{0.7}\text{Ge}_{0.3}$ alloy by pure bulk Ge; additionally, built-in biaxial stress induced by the $\text{Si}_{0.7}\text{Ge}_{0.3}$ substrate is implemented via setting the in-plane lattice constant of the system to the lattice constant of the $\text{Si}_{0.7}\text{Ge}_{0.3}$ alloy (5.5004 Å) in our atomistic calculations. This approximation will certainly introduce the differences in the conduction band offset and interface potential by alloy disorder that might reduce the QW valley splitting 2δ [marked as the dashed lines in Figs. 1(b) and 1(c)]. Considering the main purpose of this work is to demonstrate that the VS can be remarkably enhanced by engineering the (single) top interface of the Si QW alone by fixing the bottom interface to Si-QW/Ge substrate, the adopted approximation will not change our conclusions. By performing atomistic calculations, we examine VS of the Si_{40} QW/ $(\text{Ge}_m\text{Si}_m)_n$ SL barrier hybrid systems as reducing the number of SL periods n for a variety of periodic thickness $m = 2, 3, 4, 5, 6$. We indeed find that replacing two mirror-symmetric $m = 4$ SLs by one side of $m = 4$ SL degrades the VS slightly from 7.2 meV to 5 meV for a 40-ML-thick Si QW. Reducing the number of SL periods n for simplification, VS decreases gradually. Fortunately, even at the smallest number of periods ($n = 1$), VS still has a sizable value of 1.6 meV, which is large enough for developing stable spin qubits. In contrast, $m \neq 4$ SL barriers suppress the VS of Si QW to less than 1 meV. To reveal the underlying microscopic physics, we expand the Hilbert space by additionally including the miniband-edge states of the SL barrier (SL-MBS) different from the traditional valley splitting theory, which considers only the lowest two valley states in the Si QW (QW-VS) [6–11]. Based on this consideration, we establish the effective Hamiltonian model of the hybrid system. In the model, the coupling between QW-VS and SL-MBS states is treated as off-diagonal elements. After employing the Löwding partition, we obtain the reduced Hamiltonian for the two lowest valley states with the effects of SL-MBS treated as first-order perturbation [38]. It is thus straightforward to get VS of the hybrid system in a simple but intuitive formula, providing a deep insight into the significant enhancement of VS by the SL barrier. We find that the presence of the SL barrier will reduce the VS instead of enhancing it. Only the $m = 4$ SL barrier with an extremely strong coupling with Si QW valley states provides a remarkable enhancement in VS.

II. THEORETICAL METHODS

A. Atomistic calculation method

We investigate here the Si QW and GeSi SL interaction effects on the valley coupling between the two lowest Si valley states using a direct diagonalization of the band Hamiltonian $-\frac{1}{2}\nabla^2 + V(\mathbf{r})$ for the QW/SL hybrid structure described by its potential $V(\mathbf{r})$. We use for the potential of the hybrid structure a superposition of overlapping, spherical screened pseudopotential $v_\alpha(r)$ of the constituent atom [36,37],

$$V(\mathbf{r}) = \sum_n \sum_\alpha \hat{v}_\alpha(\mathbf{r} - \mathbf{R}_n - \mathbf{d}_\alpha), \quad (1)$$

where $\hat{v}_\alpha(\mathbf{r} - \mathbf{R}_n - \mathbf{d}_\alpha)$ is the screened pseudopotential containing spin-orbit interaction of atom type α at site \mathbf{d}_α in the n th primary cell \mathbf{R}_n . Considering the 4.2% lattice mismatch

between Si and Ge, a large strain exists between atomic thin Si and Ge layers in GeSi SL. We use the atomistic valence force field method [39,40] to minimize the strain energy when finding the atomic equilibrium positions. We diagonalize $-\frac{1}{2}\nabla^2 + V(\mathbf{r})$ within a plane-wave basis [36] whose size is sufficiently selected such that the weak valley coupling is accurately considered. The supercell approach combined with the periodic boundary conditions is implemented. The screened pseudopotentials $\{\hat{v}_\alpha\}$ are fitted [36] so as to remove the ‘‘LDA error’’ in the bulk crystal; they reproduce well not only the band gaps throughout the zone, but also the electron and hole effective-mass tensors, as well as the valence band and conduction band offsets between well and barrier materials, spin-orbit splittings, and GW spin-splitting in bulk materials [41]. This is described in Refs. [36,41]. This approach has been previously applied to superlattices [42,43], colloidal quantum dots [44], and Stranski-Krastanow quantum dots [45].

B. Effective Hamiltonian model

The hybrid system consists of [001]-oriented Si QW and $(\text{Ge}_m\text{Si}_m)_n$ SL barrier. These two components possess D_{2d} , C_{2v} point symmetries. The whole system is of C_1 symmetry in the QW growth direction. Symmetry allows the couplings between the QW-VS and the SL-MBS because these states share the single representation of the point group (in terms of the double group, including spin-orbit coupling). These couplings may influence the VS of the Si QW subunit. To access this influence, we expand the Hilbert space of the lowest two Si valley states [6–11] to include SL-MBS of the SL barrier and have the effective Hamiltonian for the hybrid system by introducing the coupling between QW-VS and SL-MBS states (off-diagonal elements) as follows:

$$H = \begin{bmatrix} \epsilon_0^{\text{QW}} & \delta & \lambda_1^1 & \dots & \lambda_i^1 & \dots & \lambda_n^1 \\ \delta & \epsilon_0^{\text{QW}} & \lambda_1^2 & \dots & \lambda_i^2 & \dots & \lambda_n^2 \\ \lambda_1^1 & \lambda_1^2 & \epsilon_1^{\text{SL}} & 0 & 0 & 0 & 0 \\ \dots & \dots & 0 & \dots & 0 & 0 & 0 \\ \lambda_i^1 & \lambda_i^2 & 0 & 0 & \epsilon_i^{\text{SL}} & 0 & 0 \\ \dots & \dots & 0 & 0 & 0 & \dots & 0 \\ \lambda_n^1 & \lambda_n^2 & 0 & 0 & 0 & 0 & \epsilon_{2n}^{\text{SL}} \end{bmatrix}, \quad (2)$$

where the diagonal element ϵ_0^{QW} is the average of the lowest two degenerate valley states in the Si QW. This twofold degeneracy is lifted in the energy of 2δ by the confinement potential. Therefore, the energy levels of the two Si valleys are $\epsilon_1^{\text{QW}} = \epsilon_0^{\text{QW}} - \delta$, and $\epsilon_2^{\text{QW}} = \epsilon_0^{\text{QW}} + \delta$, respectively. ϵ_i^{SL} is the energy level of i th state in $(\text{Ge}_m\text{Si}_m)_n$ SL ($i = 1, 2, \dots, 2n$). Note that each period has Δ_z and Δ_{-z} two valley states, and thus SL with n periods has $2n$ valley states. The remaining Δ_x and Δ_y valley states are neglected due to weak coupling between Δ_z and $\Delta_{x,y}$. $\lambda_i^{1,2}$ depict the interaction strengths between two Si valley states and the i^{th} state of the $(\text{Ge}_m\text{Si}_m)_n$ SL barrier. Figures 3(a) and 3(b) schematically illustrate these SL-MBS and QW-VS as well as their couplings.

The substantial space confinement in the short-period SL barrier yields energy levels of the SL-MBS much higher

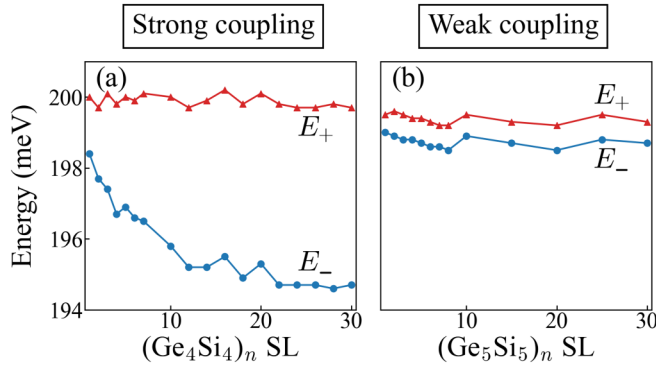


FIG. 2. Atomistic calculations predicted energy levels of the two lowest Si valley states in (a) Si₄₀ QW/(Ge₄Si₄)_n SL barrier and (b) Si₄₀ QW/(Ge₅Si₅)_n SL barrier as a function of the number of SL periods n .

than that of the QW-VS, with an energy difference being far more extensive than δ . We, therefore, can reduce the $(2 + 2n)$ -dimension effective Hamiltonian Eq. (2) to a 2×2 Hamiltonian for the lowest two Si valley states taking into account the effects of SL-MBS as first-order perturbation based on the quasidegenerate perturbation theory using the Löwding partitioning method [38]. The reduced effective Hamiltonian is thus as follows:

$$\tilde{H} = \begin{bmatrix} \tilde{H}_{11} & \tilde{H}_{12} \\ \tilde{H}_{21} & \tilde{H}_{22} \end{bmatrix} \quad (3)$$

where

$$\tilde{H}_{11} = \epsilon_0^{\text{QW}} + \sum_i^{2n} \frac{\lambda_i^1 \lambda_i^1}{\epsilon_0^{\text{QW}} - \epsilon_i^{\text{SL}}}, \quad (4a)$$

$$\tilde{H}_{22} = \epsilon_0^{\text{QW}} + \sum_i^{2n} \frac{\lambda_i^2 \lambda_i^2}{\epsilon_0^{\text{QW}} - \epsilon_i^{\text{SL}}}, \quad (4b)$$

$$\tilde{H}_{12} = \tilde{H}_{21} = \delta + \sum_i^{2n} \frac{\lambda_i^1 \lambda_i^2}{\epsilon_0^{\text{QW}} - \epsilon_i^{\text{SL}}}. \quad (4c)$$

The reduced Hamiltonian can now be diagonalized directly, and the corresponding eigenvalues of two valley states read

$$E_{\pm} = \frac{1}{2}(\tilde{H}_{11} + \tilde{H}_{22} \pm E_{\text{VS}}), \quad (5)$$

and the VS of the hybrid system is

$$E_{\text{VS}} = \sqrt{(\tilde{H}_{11} - \tilde{H}_{22})^2 + 4\tilde{H}_{12}\tilde{H}_{21}}. \quad (6)$$

If we learn $\lambda_i^{1,2}$, ϵ_0^{QW} , and ϵ_i^{SL} , we can then reproduce E_{VS} predicted from atomistic calculations according to Eq. (6), which will tell the factors' contribution to the enhancement of VS due to coupling between QW-VS and SL-MBS ($\lambda_i^{1,2}$).

III. COMPUTATIONAL RESULTS

Figure 1(c) shows atomistic pseudopotential method calculated VS of the Si₄₀ QW/(Ge_mSi_m)_n SL barrier hybrid

systems as a function of the number of SL periods n for a variety of period thickness $m = 2, 3, 4, 5, 6$. The VS of the isolated 40-ML Si QW embedded in the pure Ge barrier is 0.9 meV [represented by the dashed lines in Figs. 1(b) and 1(c)]. Interestingly, inserting just one unit of Ge₄Si₄ (i.e., $n = 1$ in the case of $m = 4$ SL barrier) into the interface between Si QW and Ge barrier, the VS is immediately enhanced to $E_{\text{VS}} = 1.6$ meV. This means we can considerably simplify the hybrid system by reducing the number of (Ge₄Si₄)_n SL periods to $n = 1$ to have a large enough VS for Si electron spin qubits [12]. Increasing the number of (Ge₄Si₄)_n SL periods from $n = 1$ to $n = 10$, E_{VS} raises rapidly from 1.6 to 4.2 meV. After that, E_{VS} grows slowly toward a saturation value of 5 meV as further increasing n . We note that this saturation value is only slightly smaller than $E_{\text{VS}} = 7.2$ meV of the original sandwich structure of the (Si)₄₀ QW/(Ge_mSi_m)₁₀ SL barrier [32] despite the former being much simpler than the latter for experimental fabrication as shown in Fig. 1(a). Whereas, in cases of $m \neq 4$ SL barriers, we see that E_{VS} is even smaller than the VS ($E_{\text{VS}} = 0.9$ meV) of the isolated Si QW in a whole range of investigated periods $n = 1 - 30$. This result is unexpected. It also implies that the enhanced E_{VS} by the $m = 4$ SL barrier is susceptible to the fluctuation of the atomic thickness in SL repeating units, which requires precisely controlled growth of Si/Ge interfaces at the atomic layer level.

We also examine the corresponding energy levels of the two lowest valley states of the hybrid systems as a function of the number of SL periods n for $m = 4$ and $m = 5$ SL barriers. Figure 2(a) shows the results for Si QW/(Ge₄Si₄)_n SL barrier hybrid system. It is interesting to see that, with the increasing the number of SL periods n , the upper level stays almost constant with a small fluctuation and the lower one goes down in energy, leading to the increase in E_{VS} , as shown in Fig. 1(c). Whereas, in the case of (Ge₅Si₅)_n SL barrier, Fig. 2(b) shows that both energy levels are insensitive to varying the number of SL periods n , yielding a period-independent VS [see Fig. 1(c)].

IV. DISCUSSION

A. The effect of the SL barrier states on VS

To understand the computationally calculated results as mentioned above, we have developed an effective Hamiltonian model as presented in the method section. However, it requires assessing $\lambda_i^{1,2}$, ϵ_0^{QW} , and ϵ_i^{SL} , which are difficult to obtain. In the following, we take further approximations. Firstly, we expect the coupling strengths between each SL state and two Si valley states to be approximately the same, i.e., $\lambda_i^1 \sim \lambda_i^2$, regarding two Si valley states have a similar envelop wave function [see Fig. 4(a)] and $2\delta \ll \epsilon_i^{\text{SL}} - \epsilon_0^{\text{QW}}$. For the sake of simplicity, we make a rough assumption that all SL-MBS have the same coupling strength to the QW-VS, i.e., $\lambda_i^1 \sim \lambda_i^2 \sim \Lambda$. As a result, we can further simplify Eqs. (5) and (6) as

$$E_{\pm} = \epsilon_0^{\text{QW}} - \Lambda^2 T \pm \frac{1}{2} E_{\text{VS}}, \quad (7a)$$

$$E_{\text{VS}} = 2|\Lambda^2 T - \delta|, \quad (7b)$$

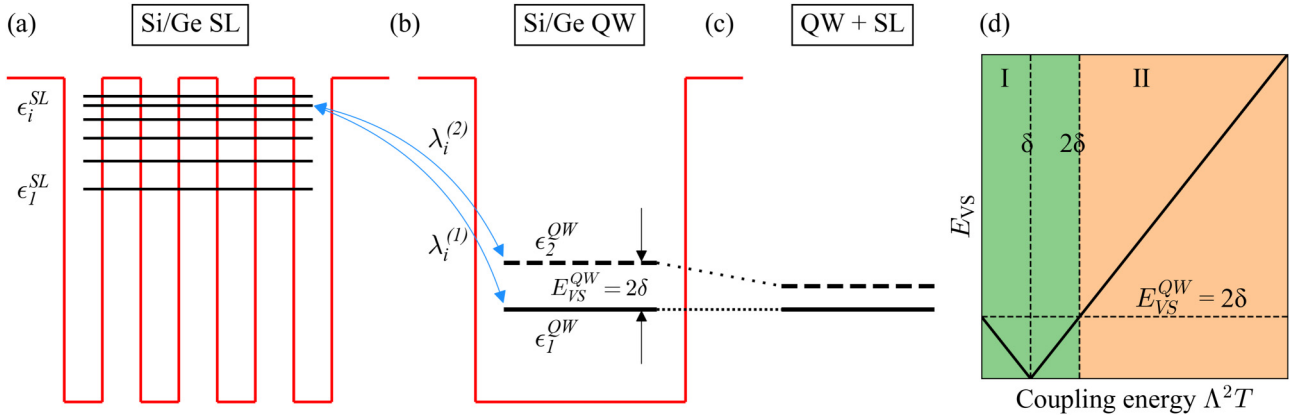


FIG. 3. (a),(b) Schematic representation of the interaction between the QW-VS and the SL-MBS. (c) Energies of the two Si valley states due to the QW/SL coupling. (d) VS as the function of the coupling energy; I is the weak coupling region, and II is the strong coupling region. Only when the coupling energy exceeds the critical value, namely $\Lambda^2 T > 2\delta$, the corresponding VS starts to be enhanced.

where

$$T \equiv \sum_i^{2n} \frac{1}{\epsilon_i^{\text{SL}} - \epsilon_0^{\text{QW}}}, \quad (8)$$

where Λ quantifies the averaged coupling strength between SL-MBS and QW-VS, and T is an energy factor representing the energy distribution of the SL-MBS relative to QW-VS. Therefore, $\Lambda^2 T$ quantifies the total QW/SL coupling strength.

It is straightforward to read from Eq. (7a) that, if $\Lambda^2 T \leq \delta$, $E_+ = \epsilon_0^{\text{QW}} + \delta - 2\Lambda^2 T$ and $E_- = \epsilon_0^{\text{QW}} - \delta$, otherwise $E_+ = \epsilon_0^{\text{QW}} - \delta$ and $E_- = \epsilon_0^{\text{QW}} + \delta - 2\Lambda^2 T$. Interestingly, we can learn that the QW/SL coupling will not alter the energy level of the lower one of the two valley states in Si QW but push down the upper one. This model result explains exactly the above observation in the atomistic calculations (Fig. 2) that there is one energy level that stays almost constant with a small fluctuation as varying the number of periods n as well as the period thickness m . It has also been schematically illustrated in Fig. 3(c). As increasing the QW/SL strength $\Lambda^2 T$ from zero to δ , the upper valley approaches toward the lower valley, resulting in the reduction in E_{VS} . At $\Lambda^2 T = \delta$, the upper valley passes the lower valley, eliminating the VS ($E_{\text{VS}} = 0$). Afterward, when further increasing the QW/SL strength $\Lambda^2 T$, the original upper valley (now becomes lower in energy) continuously goes down in energy, raising again the VS, but being still smaller than 2δ the VS of the isolated Si QW. The enhancement in VS (i.e., $E_{\text{VS}} > 2\delta$) occurs only when $\Lambda^2 T > 2\delta$. Consequently, the presence of the SL barrier is, surprisingly, suppressing the VS instead of enhancing it unless the QW/SL coupling strength is strong enough. This finding explains why the VS of hybrid systems for all $m \neq 4$ SL barriers is even smaller than that of the isolated Si QW, as shown in Fig. 1(c).

Figure 3(d) sketches that we can divide the QW/SL coupling into two regions: strong coupling ($\Lambda^2 T > 2\delta$) and weak coupling ($\Lambda^2 T \leq 2\delta$). From the results presented in Figs. 1(b) and 1(c) we learn that the $(\text{Ge}_4\text{Si}_4)_n$ SL barrier provides a strong QW/SL coupling and the remaining $m \neq 4$ $(\text{Ge}_m\text{Si}_m)_n$ SL barriers are in the weak coupling region. In the following, we attempt to unravel the physics causing the $m = 4$ SL bar-

rier to stand out clearly from the remaining $m \neq 4$ SL barriers by examining the coupling matrix Λ and energy factor T separately.

B. The coupling matrix Λ

The coupling matrix Λ is defined as: $\Lambda = \langle \psi^{\text{QW}} | \Delta V | \psi^{\text{SL}} \rangle$. The perturbation potential ΔV couples the QW valley states to the SL miniband states and is given by $\Delta V = U \Theta(z + \frac{l}{2}) \Theta(-z + \frac{l}{2})$, where l is the SL period thickness m and U is the conduction band offset between Ge and Si. Thus, we can assess the magnitude of Λ by examining the wave function overlaps around the interfaces, as shown in Fig. 4(a). Therefore, the Λ reads as follows: $\Lambda = U \int \Theta(z + \frac{l}{2}) \Theta(-z + \frac{l}{2}) \psi^{\text{SL}}(z) \psi^{\text{QW}}(z) dz = U \int_{-l/2}^{l/2} \psi^{\text{SL}}(z) \psi^{\text{QW}}(z) dz$. Reference [32] has shown that the SL barriers usually enhance the localization of wave functions of the lowest two valley states inside the Si QW layer with a much smaller leakage into the barrier in comparison with the SiGe alloy barrier. However, there is no one-to-one relationship between VS and wave-function leakage. Figure 4(a) shows that the difference in $(\text{Ge}_m\text{Si}_m)_n$ SL barriers introduces hardly a sizable change in wave functions of two valley states. In this respect, $\psi^{\text{QW}}(z)$ can be approximated as a constant A in the above integral, and the coupling matrix can be further reduced as: $\Lambda \sim AU \int_{-l/2}^{l/2} \psi^{\text{SL}}(z) dz \sim AU \int_{z_0}^{z_1} \psi^{\text{SL}}(z) dz \propto \int_{z_0}^{z_1} \psi^{\text{SL}}(z) dz$, which is namely the evanescent integral of the $(\text{Ge}_m\text{Si}_m)_n$ SL wave functions. Considering the energy factor U is the same in the evanescent integrals for different $(\text{Ge}_m\text{Si}_m)_n$ SL, we can factor it out. Dropping the energy factor U is reasonable since we only care about the relative magnitudes among different SLs. For the integral range, we choose z_0 and z_1 as 0 and a , with coordinate origin at the position of the interface between the Si QW and the nearest neighboring Ge_m barrier. a is the lattice constant of the Si.

The evanescent integrals for different $(\text{Ge}_m\text{Si}_m)_5$ SL barriers are given in Fig. 4(b). One can see that the magnitude of Λ decreases as the SL period thickness m increases. Note that, in SLs made by semiconductors, the electron states in

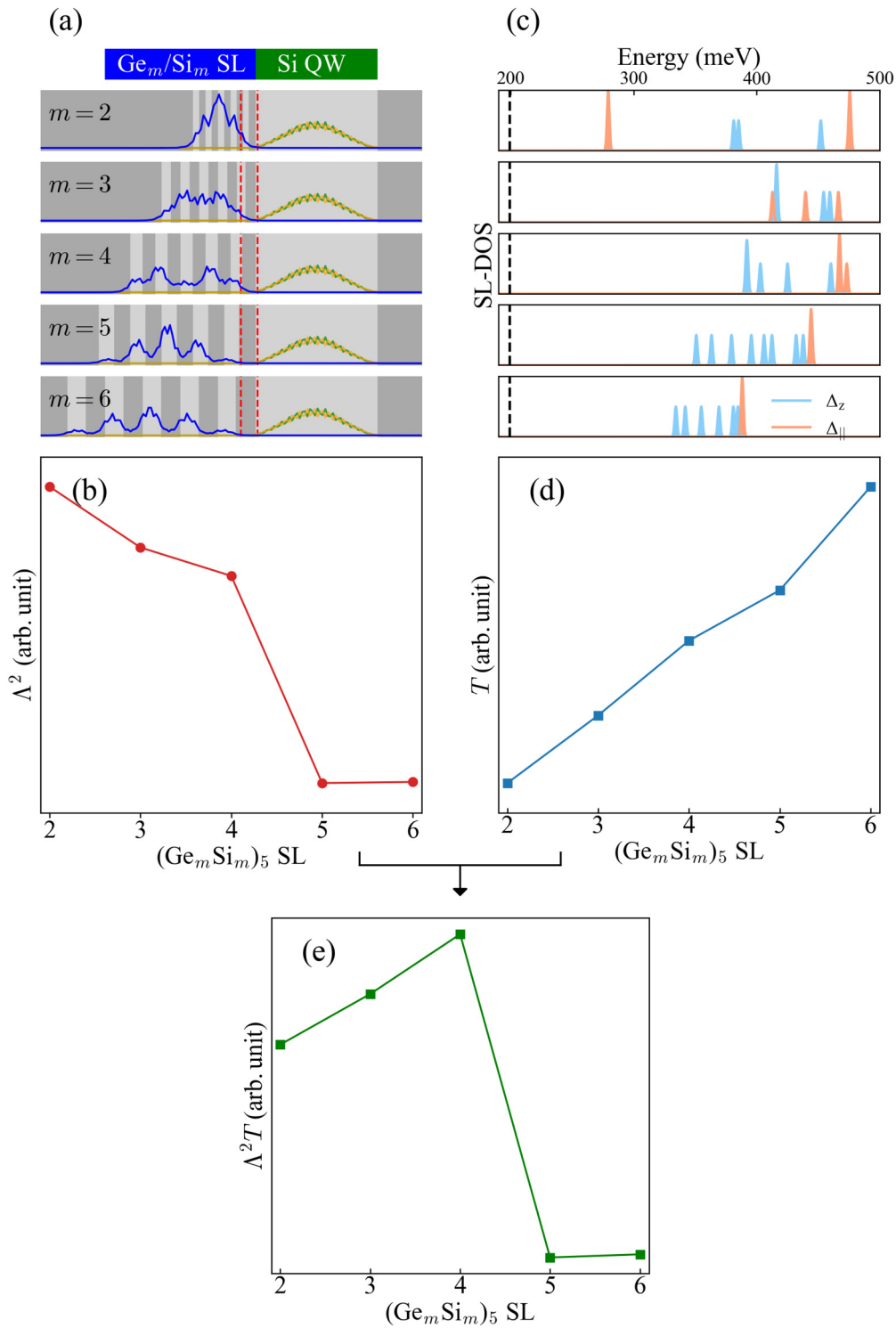


FIG. 4. (a) Wave-function overlap between the QW-VS and the SL-MBS around the interface. The red dashed lines mark their overlap region. (b) The estimated coupling matrices for different $\text{Ge}_m\text{Si}_m \text{ SL}$. (c) Energy spectrum of different $\text{Ge}_m\text{Si}_m \text{ SL}$ (with SL period of 5). The reciprocal-space characters are quantified using the majority representation approach [46] combined with the weight functions [47]. The black dashed lines mark the position of Si valley states in isolated Si QW. (d) The calculated energy factors T for different $\text{Ge}_m\text{Si}_m \text{ SL}$. (e) The total coupling strength $\Lambda^2 T$ between different $\text{Ge}_m\text{Si}_m \text{ SL}$ and Si QW.

neighboring QWs can interact as the barrier width decreases to a sufficient narrow thickness. The corresponding discrete energy levels confined inside QWs broaden into energy bands known as minibands, which are very narrow in energy com-

pared to bulk energy bands [48]. In the Si/Ge heterostructures, it is well known that the electron states are localized inside the Si layer [49]. Thus, thicker Ge sublayers of the $(\text{Ge}_m\text{Si}_m)_n \text{ SL}$ cause SL miniband states to be less expanded and create

narrower minibands. Furthermore, the thicker Si_m sublayer will also give the electron states more space confinement, making their wave functions more localized inside Si sublayers. Figure 4(a) indeed shows that the wave function in $(\text{Ge}_6\text{Si}_6)_n$ SL is the most localized while the wave function in $(\text{Ge}_2\text{Si}_2)_n$ SL is the most extended. Therefore, electron states of SL with larger m have less probability of tunneling into the Si QW region. In this respect, a smaller coupling matrix Λ is expected for $(\text{Ge}_m\text{Si}_m)_n$ SL with larger m , as shown in Fig. 4(b) based on a rough evaluation from the evanescent integral.

C. The energy factor T

We now turn to evaluate the dependence of the energy factor T on the period thickness m of the $(\text{Ge}_m\text{Si}_m)_n$ SL barrier in hybrid systems. To do so, we have also computed the unperturbed energy levels ϵ_0^{QW} and ϵ_i^{SL} of isolated Si QW and five-period $(\text{Ge}_m\text{Si}_m)_5$ SL, respectively, by carrying out atomistic SEPM calculations. Both isolated Si QW and five-period $(\text{Ge}_m\text{Si}_m)_5$ SL are separately embedded within the pure Ge matrix. Figure 4(c) shows the atomistic calculations predicted results. One can see that, as the period thickness is getting thinner (or m decreases), the SL energy levels ϵ_i^{SL} raise and are going far away from the Si QW valley level ϵ_0^{QW} . This raising in the SL energy levels is attributed to the enhanced quantum confinement effect. The energy spacing between SL energy levels ϵ_i^{SL} is also getting larger, responsible for a wider miniband width. We sum up the SL energy levels relative to ϵ_0^{QW} according to Eq. (8), giving rise to the energy factor T , which is shown in Fig. 4(d) as a function of SL period thickness m . One can see that T gets larger almost linearly as increasing the SL period thickness m . It is straightforward to learn that this linear increase in T is due to going down in energy of all ϵ_i^{SL} relative to ϵ_0^{QW} .

Furthermore, if the number of SL periods n is infinite, the discrete energy levels in the SL form minibands. The summation in T term can then be approximated by the integral over a fixed energy interval from miniband bottom (ϵ_1^{SL}) to miniband top ($\epsilon_{2n}^{\text{SL}}$): $T \equiv \sum_i \frac{1}{\epsilon_i^{\text{SL}} - \epsilon_0^{\text{QW}}} \propto \int_{\epsilon_1^{\text{SL}}}^{\epsilon_{2n}^{\text{SL}}} \frac{1}{\epsilon_i^{\text{SL}} - \epsilon_0^{\text{QW}}} d\epsilon = \ln\left(\frac{\epsilon_{2n}^{\text{SL}} - \epsilon_0^{\text{QW}}}{\epsilon_1^{\text{SL}} - \epsilon_0^{\text{QW}}}\right)$. This approximation shows that, in addition to the absolute energy level positions, the miniband width is also an important parameter. Wider miniband width $\epsilon_{2n}^{\text{SL}} - \epsilon_1^{\text{SL}}$ occurring in smaller period thickness will give larger T and thus larger VS, which compensates partially the reduction in T and thus VS induced by energy level shifting up due to strong confinement in narrow period thickness.

D. Nonmonotonic dependence of coupling strength $\Lambda^2 T$ on SL period thickness m .

So far, we have shown that by decreasing the periodic thickness of the SL barriers but keeping the number of periods constant, the coupling matrix Λ^2 is going to become bigger, and the energy factor T will get smaller for hybrid systems. Figure 4(e) shows that the opposite trends in Λ^2 and T render their product the total coupling strength $\Lambda^2 T$ to be a nonmonotonic function as varying the periodic thickness m with a sharp peak occurs at $m = 4$. This result agrees with the atomistic calculation where the Ge_4Si_4 SL induce the largest

VS, as shown in Fig. 1(a). Therefore, we have illustrated that the competition between the coupling matrix and energy factor makes $m = 4$ SL barrier defeating the remaining $m \neq 4$ SL barriers to possess alone the strong coupling. In contrast, the hybrid systems associated with the remaining $m \neq 4$ SL barriers are in the weak coupling region, with E_{VS} being smaller than the VS of the isolated Si QW, which is 0.96 meV for an isolated 40-ML Si QW embedded in the pure Ge matrix. In particular, the trend of VS with SL period thickness m in Fig. 1(b) and one of estimated coupling energy with SL period thickness m in Fig. 4(e) do not exactly agree. This is mainly caused by the approximation we have taken in estimating the coupling energy. It should be emphasized that our aim is to highlight the nonmonotonic character of the variation of the coupling energy with the SL period thickness m .

E. Physics underlying the further improvement of VS by increasing the $m = 4$ SL period.

We can now explain why only the $(\text{Ge}_4\text{Si}_4)_n$ SL barrier will continuously enhance the VS by increasing the number of SL periods n ; whereas the remaining $m \neq 4$ SL barriers lack such enhancement, as shown in Fig. 1(c). Because the number of SL periods quantifies the total number of quantum states in the miniband [50], the number of the valley states composing the SL miniband grows doubly as increasing the number of SL periods n , which has been explained in the text above Eq. (2). According to Eq. (8), a more significant number of SL periods n gives a more considerable energy factor T . On the other hand, increasing the SL periods is expected to reduce the component of wave functions penetration into the Si QW, which will suppress the coupling matrix Λ . Figure 5 shows the spatial distributions of the two lowest SL-MBS in $(\text{Ge}_m\text{Si}_m)_n$ SL with varying m and n . One can observe a unique feature of the $m = 4$ SL: the lowest energy ground state is p like as it has one node in its envelope function. Whereas, remaining $m \neq 4$ SLs have an s -like ground state as usual. Figure 5 exhibits that the p -like ground state in the $m = 4$ SL guarantees more distributions of wave functions at the two terminated interfaces. That, in turn, ensures the component penetration into the Si QW, equally the coupling matrix Λ , is unchanged as increasing n . In contrast, the s -like ground state in the remaining $m \neq 4$ SLs is distributed mainly inside the SL with tails on the two terminated interfaces. In these $m \neq 4$ SLs, increasing the number of SL periods will increase the component inside the SL and thus reduce the component penetration into the Si QW. Subsequently, as the SL period increases, the coupling matrix Λ decreases for $m \neq 4$ SLs. The rise of T and decrease of Λ may make the E_{VS} a product of Λ and T unchanged in $m \neq 4$ SLs, as shown in Fig. 1(c). However, the increased T and unchanged Λ make the E_{VS} enhanced continuously as increasing n in $m = 4$ SL.

V. CONCLUSION

To make fabrication feasible, we have remarkably simplified the originally designed structure of the Si QW sandwiched by two symmetric Ge/Si SLs with substantially enhanced valley splitting E_{VS} exceeding 9 meV [32]. The simplified structure is engineered by laying out the Si QW

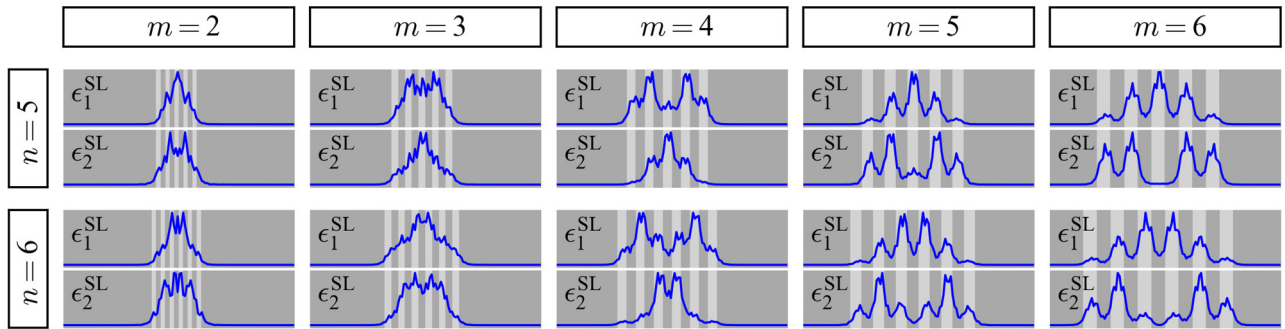


FIG. 5. Atomistic calculated wave functions of two lowest SL-MBS in $(\text{Ge}_m\text{Si}_m)_n$ SL with variant m and n .

on the SiGe substrate and then capping a $(\text{Ge}_4\text{Si}_4)_n$ SL barrier on top of the Si QW. By performing the sophisticated atomistic-pseudopotential calculations, we predicted that such simplification leads to a small sacrifice on E_{VS} , reducing it from the original 8.7 to 5.2 meV. We reduce the SL period n in the $(\text{Ge}_4\text{Si}_4)_n$ barrier to further simplify the structure. In that case, E_{VS} decreases gradually but still has a large enough value of $E_{\text{VS}} = 1.6$ meV needed for electron spin qubits. Interestingly, the $m = 4$ SL barrier is unique because the E_{VS} is less than 1 meV in structures associated with $m \neq 4$ SL barriers. To reveal the underlying microscopic physics, we have developed an effective Hamiltonian model of the simplified structure and thus obtained E_{VS} in a simple but intuitive formula, providing insight into the enhancement of VS by SL barrier. Surprisingly, we found that the presence of the SL barrier is usually suppressing the E_{VS} instead of enhancing unless the QW/SL coupling strength is strong enough. We demonstrated that only the $(\text{Ge}_4\text{Si}_4)_n$ SL barrier has a strong coupling between QW and SL and thus gives rise to significantly enhanced E_{VS} . In contrast, the remaining $m \neq 4$ SL barriers have weak coupling and thus yield E_{VS} even smaller than the corresponding isolated Si QW value. Our results provide an effective, more importantly, easily fabricated approach to fulfill the large VS in Si that makes Si spin qubit gain new momentum in pursuing the general quantum computation.

ACKNOWLEDGMENTS

The work was supported by the National Science Fund for Distinguished Young Scholars under Grant No. 11925407, the Basic Science Center Program of the National Natural Science Foundation of China (NSFC) under Grant No. 61888102, and the Key Research Program of Frontier Sciences, CAS under Grant No. ZDBS-LY-JSC019 and CAS Project for Young Scientists in Basic Research under Grant No. YSBR-026. Z.-G.S. was also supported by the National Key Research and Development Program of China under Grant No. 2021YFB2800304.

APPENDIX A: EFFECT OF QW WIDTH ON THE VS IN OUR PROPOSED DEVICE TOPOLOGY

We perform the atomistic calculations for a 40-ML (5.4-nm) thick Si QW. However, in practice, for easier device fabrication, the Si QW usually has a thicker well width, typically 8 nm [25–31]. The VS is known to decrease as the QW

width increases [7–11,32,51]. The decreasing VS is due to the reduced value of the valley wave function at the interface caused by the weakening of the quantum confinement effect in the thicker QW. In the present work, we focus on the relative magnitudes between the VS induced by different Ge_mSi_m SL barriers, for which we need to fix the QW thickness. However, the increase of the QW width will uniformly change the VS in different Si QW/ Ge_mSi_m -SL hybrid structures so that the optimal period thickness m would not change due to the increase of the QW width. To make our conclusions more reliable, we give the results of atomistic calculations for 10-nm-thick Si QW, which are presented in Fig. 6. We see that SL period thickness m is still 4 ML to have a significant enhancement on VS over the remaining SL period thickness although its enhanced VS is reduced from 5 meV in the case of 5.4-nm-thick Si QW to 0.5 meV in the 10-nm-thick QWs when SL having period n of 20. Therefore, we safely drew the conclusions based on the 5.4-nm-thick Si QW.

APPENDIX B: IMPACT OF INTERFACE ROUGHNESS AND ATOMIC STEP EDGES ON OUR PROPOSED DEVICE TOPOLOGY

The VS is known to be quite sensitive to atomistic details. We evaluate the impact of interface roughness on the VS in

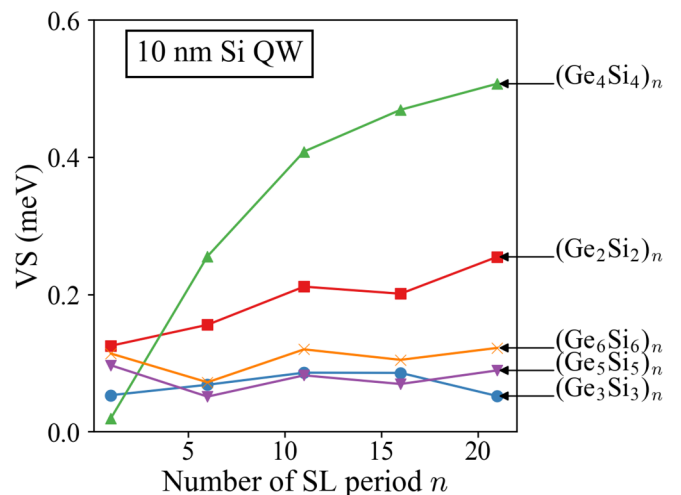


FIG. 6. Calculated E_{VS} of 10 nm Si QW/ $(\text{Ge}_m\text{Si}_m)_n$ SL barrier hybrid systems as a function of the number of SL periods n for period thickness $m = 2, 3, 4, 5, 6$.

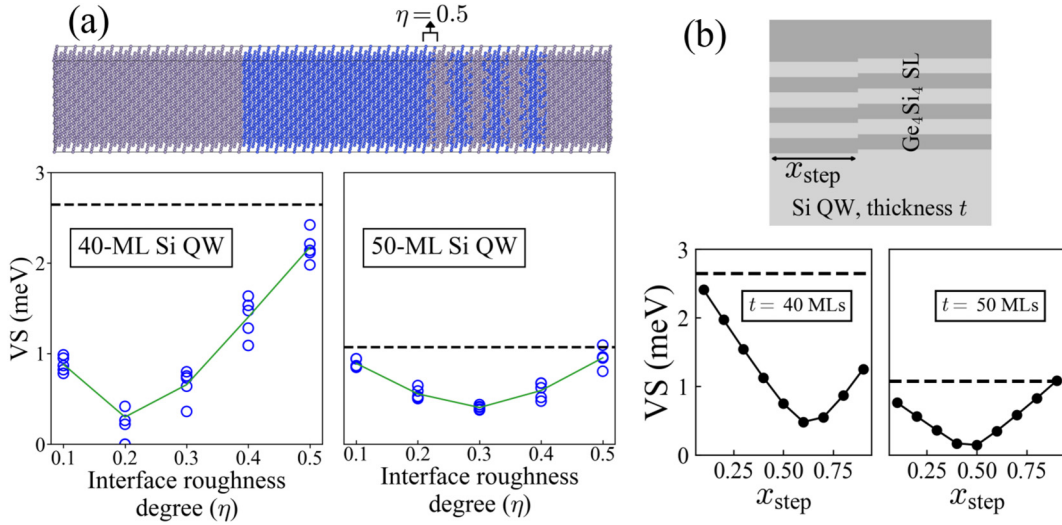


FIG. 7. (a) Interface roughness effect. Si QW/(Ge₄Si₄)₃ SL structure in the presence of interface roughness η is shown at the top. In order to evaluate the interface roughness, we replace the pure Ge by Ge _{η} Si_{1- η} alloy and pure Si by Si _{η} Ge_{1- η} at the Ge/Si interface. The maximum degree of interface roughness is $\eta = 0.5$. Two lower graphs show VS as the function of η for 40-ML and 50-ML Si QW, respectively. The black dashed lines indicate the VS values with ideal interface. Five empty circles for a give roughness η represent the results of five different alloy configurations at the interface. Green solid lines denote the VS values after averaging over different configurations. (b) Atomic step edge effect. Schematic diagram of Si QW/(Ge₄Si₄)₃ SL with one interface step at each Ge/Si hetero-interface. x_{step} quantifies the interface step positions in the x direction. Calculated VS as the function of x_{step} for Si QW with well width of 40 and 50 ML are displayed separately at the lower side.

Si QW/Ge₄Si₄ SL in Fig. 7(a). Overall, interface roughness reduces the VS as usual. Interestingly, the interface roughness induced VS degradation in our device topology does not maximize when the individual Ge/Si hetero-interface has the most considerable degree ($\eta = 0.5$) of roughness but an intermediate one. This nonmonotonic behavior stems from the new pseudo-ordered periodic structure i.e., (Ge_{0.5}Si_{0.5})₂/Ge₂/(Ge_{0.5}Si_{0.5})₂/Si₂... in the $\eta = 0.5$ case. The nominal maximum disorder happens at the middle η value. The roughness among different Ge/Si heterointerface is typically uncorrelated, thus disrupting the SL's periodic structure. Accordingly, SL defect states appear. In this way, the localization of the SL defect states causes the decrease of coupling strength between QW and SL. That is why the interface roughness or period thickness m fluctuations in the Ge _{m} Si _{m} SL decrease the VS. In contrast, the restoration of the “periodic structure”, which is technically not that periodic but is “pseudo-ordered”, in the $\eta = 0.5$ case adds up to the reduction in the number of SL defect states, which in turn relieves the VS suppression caused by the interface roughness. We assess the influence of interface steps on the VS in Si QW/Ge₄Si₄ SL hybrid structure in Fig. 7(b). Only the single interface step case is shown here. Similar VS behaviors are presented in the multiple interface step case provided that the different in-plane sections (having different well width) are divided by the interface steps, and have the same portion as in the single case. To be specific, the VS is the same in the following two cases: (1) A single interface step separates the whole structure into Si QW($t = t_0$)/Ge₄Si₄ SL and Si QW($t = t_0 + 1$)/Ge₄Si₄ SL with ratios of 0.6 and 0.4 in the x direction. (2) Two interface steps split the whole structure into Si QW($t = t_0$)/Ge₄Si₄ SL, Si QW($t = t_0 + 1$)/Ge₄Si₄ SL and Si QW($t = t_0$)/Ge₄Si₄ SL with ratios of 0.2, 0.4, and 0.4.

APPENDIX C: EFFECT OF ELECTRIC FIELD

VS enhancement [9,11,52,53] by the out-of-plane electric field E_z is typically visible [12,24] in MOS-based devices where the electron is strongly confined to the oxide interface. A tunable VS that linearly depends on E_z has been reported [12,24] in MOS devices. However, to the best of our knowledge, in Si/SiGe heterojunction devices, VS is rarely modified by E_z , but rather the VS is changed in the two-dimensional electron gas at the Si/SiGe interface by modulating the Landau level occupation through the application of an

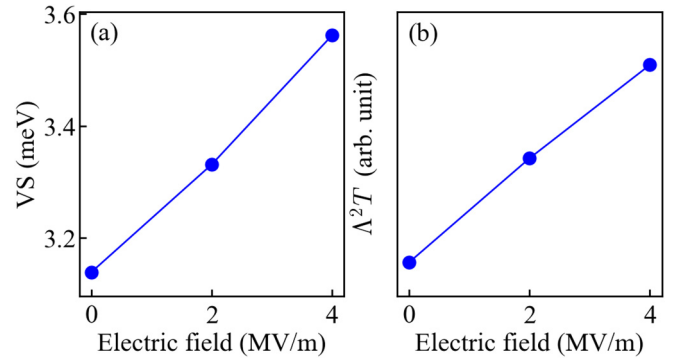


FIG. 8. (a) Atomistic calculations of VS as function of electric field in Si QW (40 ML)/(Ge₄Si₄)₅-SL hybrid structure. Electric field drives the valley states close to the (Ge₄Si₄)₅-SL. (b) Calculated coupling strength $\Lambda^2 T$ presented in the linear scale, $\Lambda^2 T = \sum_{i=1}^n \frac{|\langle \psi_i^{\text{SL}} | \Delta V | \psi_i^{\text{QW}} \rangle|^2}{\epsilon_{\text{SL}} - \epsilon_{\text{QW}}}$, as function of electric field in 5.4-nm-thick Si QW/(Ge₄Si₄)₅-SL hybrid structure by effective mass envelope function method. The electric field drives the valley states close to (Ge₄Si₄)₅-SL.

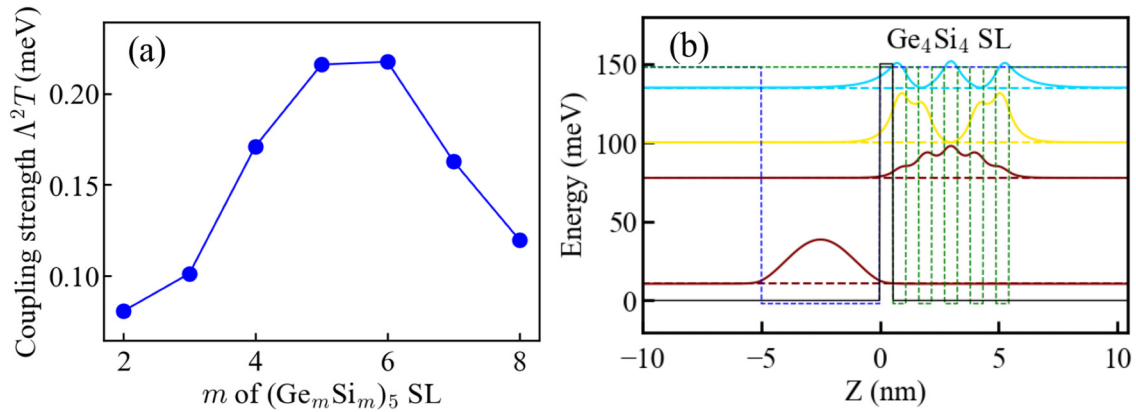


FIG. 9. (a) Coupling strength between Si QW and $(\text{Ge}_m\text{Si}_m)_5$ SL as the function of SL period thickness m calculated via the envelope function method. $\Lambda^2 T = \sum_{i=1}^n \frac{|\langle \psi_i^{\text{SL}} | \Delta V | \psi_i^{\text{QW}} \rangle|^2}{\epsilon_i^{\text{SL}} - \epsilon_i^{\text{QW}}}$, the summation runs over SL miniband bound states. (b) Envelope functions and eigen energies of both Si QW valley states and SL miniband bound states in case of Si QW/ $(\text{Ge}_m\text{Si}_m)_5$ -SL hybrid system. The perturbation potential ΔV is indicated by the black solid line.

out-of-plane magnetic field [26,27]. Recent work [29] has attempted to tune VS by electric field in Si/SiGe heterojunction devices. However, the researchers were unable to tune VS by E_z due to the limitation of the relatively weak E_z . Instead, they found that they could tune VS by electric field by modulating the horizontal movement of QD at the heterojunction interface relative to the interface step. In any case, a few MV/m of E_z can be held in the Si/SiGe heterojunction device, such that it is theoretically possible to achieve the adjustment of VS by changing E_z . For this purpose, we have considered the effect of E_z on VS in the Si QW/SiGe-SL structure. The results of the atomistic calculations are shown in Fig. 8(a), where it can be seen that VS also increases linearly with E_z . It should be noted that in the Si QW/SiGe-SL structure, there are two main mechanisms for the VS enhancement. First, E_z increases the original valley coupling 2δ caused by the scattering of the interface potential. This enhancement is due to the electric field that increases the electron penetration depth in the barrier thus increasing the 2δ . Second, E_z can alter the coupling energy $\Lambda^2 T$ between Si QW and SiGe SL. In order to quantify the effect of E_z on the magnitude of this coupling, we calculated the coupling energy between Si QW and SiGe SL using the effective mass envelope function method, and the results are shown in Fig. 8(b). It can be seen that the coupling energy increases when E_z is applied to drive the Si QW valley states close to the QW/SL interface. Moreover, the coupling energy increases linearly with the magnitude of E_z . Combining these two mechanisms, E_z enhances VS in the QW/SiGe-SL structure.

APPENDIX D: COUPLING STRENGTH CALCULATED BY THE EFFECTIVE MASS ENVELOPE FUNCTION METHOD

In Sec. IV D, we attribute the reason behind the maximum valley splitting induced by the $m = 4$ SL to the nonmonotonic dependence of coupling strength $\Lambda^2 T$ on SL period thickness m which originates from the competition between the decrease of coupling matrix Λ and increase in the energy factor T involved in the QW/SL interaction when widening the SL period thickness m . To further confirm the nonmonotonic dependence of the coupling strength on the SL period thickness m , we also evaluate the coupling strengths employing the effective mass envelope function method. In our envelope function calculations, we first obtain the envelope functions $(\psi_1^{\text{QW}}, \psi_i^{\text{SL}})$ and eigenenergies $(\epsilon_1^{\text{QW}}, \epsilon_i^{\text{SL}})$ of both isolated Si QW and Ge_mSi_m SL, respectively, results for Si QW/ $(\text{Ge}_4\text{Si}_4)_5$ -SL are shown in Fig. 9(b) as an example. Then we explicitly calculate the coupling strength $\Lambda^2 T$. Figure 9(a) shows the calculated results of the coupling strengths using effective mass method. We reproduce the turning point although the critical point deviates from the $m = 4$ predicted by the more sophisticated atomistic pseudopotential method. This discrepancy is owing to the continuous envelope function model fails to describe the microscopic details that the atomistic pseudopotential method can handle. Besides, the inaccuracy of wave functions obtained for the Ge_mSi_m with atomic-scale periodic thickness m through the effective mass envelope function method also catalyzes the disparity.

- [1] F. A. Zwanenburg, A. S. Dzurak, A. Morello, M. Y. Simmons, L. C. L. Hollenberg, G. Klimeck, S. Rogge, S. N. Coppersmith, and M. A. Eriksson, *Rev. Mod. Phys.* **85**, 961 (2013).
- [2] T. D. Ladd and M. S. Carroll, in *Encyclopedia of Modern Optics (Second Edition)*, edited by B. D. Guenther and D. G. Steel (Elsevier, Oxford, 2018), pp. 467–477.
- [3] C. Tahan and R. Joynt, *Phys. Rev. B* **89**, 075302 (2014).

- [4] T. Ando, A. B. Fowler, and F. Stern, *Rev. Mod. Phys.* **54**, 437 (1982).
- [5] D. P. DiVincenzo, *Fortschr. Phys.* **48**, 771 (2000).
- [6] F. J. Ohkawa and Y. Uemura, *J. Phys. Soc. Jpn.* **43**, 917 (1977).
- [7] T. B. Boykin, G. Klimeck, M. Friesen, S. N. Coppersmith, P. von Allmen, F. Oyafuso, and S. Lee, *Phys. Rev. B* **70**, 165325 (2004).

- [8] M. O. Nestoklon, L. E. Golub, and E. L. Ivchenko, *Phys. Rev. B* **73**, 235334 (2006).
- [9] M. Friesen, S. Chutia, C. Tahan, and S. N. Coppersmith, *Phys. Rev. B* **75**, 115318 (2007).
- [10] A. Valavanis, Z. Ikonić, and R. W. Kelsall, *Phys. Rev. B* **75**, 205332 (2007).
- [11] A. L. Saraiva, M. J. Calderón, X. Hu, S. Das Sarma, and B. Koiller, *Phys. Rev. B* **80**, 081305(R) (2009).
- [12] C. H. Yang, A. Rossi, R. Ruskov, N. S. Lai, F. A. Mohiyaddin, S. Lee, C. Tahan, G. Klimeck, A. Morello, and A. S. Dzurak, *Nat. Commun.* **4**, 2069 (2013).
- [13] L. Petit, J. M. Boter, H. G. J. Eenink, G. Droulers, M. L. V. Tagliaferri, R. Li, D. P. Franke, K. J. Singh, J. S. Clarke, R. N. Schouten, V. V. Dobrovitski, L. M. K. Vandersypen, and M. Veldhorst, *Phys. Rev. Lett.* **121**, 076801 (2018).
- [14] B. Koiller, X. Hu, and S. Das Sarma, *Phys. Rev. Lett.* **88**, 027903 (2001).
- [15] D. Culcer, L. Cywiński, Q. Li, X. Hu, and S. Das Sarma, *Phys. Rev. B* **80**, 205302 (2009).
- [16] R. Maurand, X. Jehl, D. Kotekar-Patil, A. Corna, H. Bohuslavskyi, R. Laviéville, L. Hutin, S. Barraud, M. Vinet, M. Sanquer, and S. De Franceschi, *Nat. Commun.* **7**, 13575 (2016).
- [17] W. Huang, C. H. Yang, K. W. Chan, T. Tantt, B. Hensen, R. C. C. Leon, M. A. Fogarty, J. C. C. Hwang, F. E. Hudson, K. M. Itoh, A. Morello, A. Laucht, and A. S. Dzurak, *Nature (London)* **569**, 532 (2019).
- [18] T. F. Watson, S. G. J. Philips, E. Kawakami, D. R. Ward, P. Scarlino, M. Veldhorst, D. E. Savage, M. G. Lagally, M. Friesen, S. N. Coppersmith, M. A. Eriksson, and L. M. K. Vandersypen, *Nature (London)* **555**, 633 (2018).
- [19] C. H. Yang, R. C. C. Leon, J. C. C. Hwang, A. Saraiva, T. Tantt, W. Huang, J. Camirand Lemyre, K. W. Chan, K. Y. Tan, F. E. Hudson, K. M. Itoh, A. Morello, M. Pioro-Ladrière, A. Laucht, and A. S. Dzurak, *Nature (London)* **580**, 350 (2020).
- [20] L. Petit, H. G. J. Eenink, M. Russ, W. I. L. Lawrie, N. W. Hendrickx, S. G. J. Philips, J. S. Clarke, L. M. K. Vandersypen, and M. Veldhorst, *Nature* **580**, 355 (2020).
- [21] J. Klinovaja, D. Stepanenko, B. I. Halperin, and D. Loss, *Phys. Rev. B* **86**, 085423 (2012).
- [22] J. M. Taylor, H.-A. Engel, W. Dür, A. Yacoby, C. M. Marcus, P. Zoller, and M. D. Lukin, *Nat. Phys.* **1**, 177 (2005).
- [23] J. Levy, *Phys. Rev. Lett.* **89**, 147902 (2002).
- [24] J. K. Gamble, P. Harvey-Collard, N. T. Jacobson, A. D. Baczewski, E. Nielsen, L. Maurer, I. Montañó, M. Rudolph, M. S. Carroll, C. H. Yang, A. Rossi, A. S. Dzurak, and R. P. Muller, *Appl. Phys. Lett.* **109**, 253101 (2016).
- [25] D. M. Zajac, T. M. Hazard, X. Mi, K. Wang, and J. R. Petta, *Appl. Phys. Lett.* **106**, 223507 (2015).
- [26] S. Goswami, K. A. Slinker, M. Friesen, L. M. McGuire, J. L. Truitt, C. Tahan, L. J. Klein, J. O. Chu, P. M. Mooney, D. W. van der Weide, R. Joynt, S. N. Coppersmith, and M. A. Eriksson, *Nat. Phys.* **3**, 41 (2007).
- [27] B. P. Wuetz, M. P. Losert, A. Tosato, M. Lodari, P. L. Bavdaz, L. Stehouwer, P. Amin, J. S. Clarke, S. N. Coppersmith, A. Sammak, M. Veldhorst, M. Friesen, and G. Scappucci, *Phys. Rev. Lett.* **125**, 186801 (2020).
- [28] X. Mi, C. G. Péterfalvi, G. Burkard, and J. R. Petta, *Phys. Rev. Lett.* **119**, 176803 (2017).
- [29] A. Hollmann, T. Struck, V. Langrock, A. Schmidbauer, F. Schauer, T. Leonhardt, K. Sawano, H. Riemann, N. V. Abrosimov, D. Bougeard, and L. R. Schreiber, *Phys. Rev. Applied* **13**, 034068 (2020).
- [30] M. G. Borselli, R. S. Ross, A. A. Kiselev, E. T. Croke, K. S. Holabird, P. W. Deelman, L. D. Warren, I. Alvarado-Rodriguez, I. Milosavljevic, F. C. Ku, W. S. Wong, A. E. Schmitz, M. Sokolich, M. F. Gyure, and A. T. Hunter, *Appl. Phys. Lett.* **98**, 123118 (2011).
- [31] F. Borjans, D. M. Zajac, T. M. Hazard, and J. R. Petta, *Phys. Rev. Applied* **11**, 044063 (2019).
- [32] L. Zhang, J.-W. Luo, A. Saraiva, B. Koiller, and A. Zunger, *Nat. Commun.* **4**, 2396 (2013).
- [33] G. Trimarchi, *J. Semicond.* **39**, 071004 (2018).
- [34] X. Zhang and J. Xia, *J. Semicond.* **39**, 071002 (2018).
- [35] L. Wang and A. Zunger, *J. Chem. Phys.* **100**, 2394 (1994).
- [36] L.-W. Wang and A. Zunger, *Phys. Rev. B* **51**, 17398 (1995).
- [37] L.-W. Wang, J. Kim, and A. Zunger, *Phys. Rev. B* **59**, 5678 (1999).
- [38] R. Winkler, *Spin-orbit Coupling Effects in Two-Dimensional Electron and Hole Systems* (Springer, Berlin, 2003).
- [39] C. Pryor, J. Kim, L. W. Wang, A. J. Williamson, and A. Zunger, *J. Appl. Phys.* **83**, 2548 (1998).
- [40] A. J. Williamson, L. W. Wang, and A. Zunger, *Phys. Rev. B* **62**, 12963 (2000).
- [41] J.-W. Luo, G. Bester, and A. Zunger, *Phys. Rev. Lett.* **102**, 056405 (2009).
- [42] R. Magri and A. Zunger, *Phys. Rev. B* **65**, 165302 (2002).
- [43] L.-W. Wang, A. Franceschetti, and A. Zunger, *Phys. Rev. Lett.* **78**, 2819 (1997).
- [44] J. M. An, A. Franceschetti, S. V. Dudiy, and A. Zunger, *Nano Lett.* **6**, 2728 (2006).
- [45] J.-W. Luo, G. Bester, and A. Zunger, *New J. Phys.* **11**, 123024 (2009).
- [46] L.-W. Wang, L. Bellaiche, S.-H. Wei, and A. Zunger, *Phys. Rev. Lett.* **80**, 4725 (1998).
- [47] J.-W. Luo, A. Franceschetti, and A. Zunger, *Phys. Rev. B* **78**, 035306 (2008).
- [48] P. Yu and M. Cardona, *Fundamentals of Semiconductors: Physics and Materials Properties*, 4th ed. (Springer, Berlin, 2010).
- [49] M. d'Avezac, J.-W. Luo, T. Chanier, and A. Zunger, *Phys. Rev. Lett.* **108**, 027401 (2012).
- [50] B. Gerald, *Wave Mechanics Applied to Semiconductor Heterostructures* (Wiley, New York, 1990), pp. 18–26.
- [51] F. J. Ohkawa, *Solid State Commun.* **26**, 69 (1978).
- [52] T. B. Boykin, G. Klimeck, M. A. Eriksson, M. Friesen, S. N. Coppersmith, P. von Allmen, F. Oyafuso, and S. Lee, *Appl. Phys. Lett.* **84**, 115 (2004).
- [53] A. Hosseinkhani and G. Burkard, *Phys. Rev. Research* **2**, 043180 (2020).